ENERGY QUIPSYS

Energy Equipment and Systems

Exergy, exergoeconomic and exergoenvironmental studies and optimization of a novel triple-evaporator refrigeration cycle with dual-nozzle ejector using low GWP refrigerants

Authors

Sahar Nazer [a]
Fateme Ahmadi Boyaghchi [a*]

[a] Department of Mechanical Engineering, Faculty of Engineering & Technology, Alzahra University, Deh-Vanak, Tehran, Iran

ABSTRACT

In this work, a novel dual-nozzle ejector enhanced triple-evaporator refrigeration cycle (DETRC) without separator is proposed to improve the performance of the conventional ejector one (CETRC). The performance of DETRC is analyzed and compared with CETRC in term of energy coefficient of performance (COP_{en}). Under given operating conditions, the COP_{en} improvement of the novel cycle could reach about 24.35% which shows the excellent energy-saving potential of DETRC in comparison with CETRC. Then, a comprehensive comparison between R717, R600a, R1234yf and R290 as low global warming potential (GWP) refrigerants of DETRC is conducted from the energy, exergy, economic and environmental impact (EI) aspects. It is observed that R717 gives better energetic and exergetic performances by 3.21 and 0.583 and R1234yf causes the lowest total product cost and EI rates of 8.186 \$/h and 0.665 Pts/h, respectively for DETRC. Moreover, increasing the high evaporating temperature improves all desired performances of DETRC, simultaneously due to the reduction of compressor consumed power. Finally, a multi-objective optimization based on an evolutionary algorithm and LINMAP decision making are carried out to ascertain the optimum exergetic, economic and EI performances of DETRC for each refrigerant.

1. Introduction

Vapor compression refrigeration cycle (VRC) contributes considerable energy consumption in the world and, thus its COP_{en} improvement is of paramount importance for energy-saving and mitigation of the environmental problems [1]. Adopting appropriate refrigerants is one method of enhancing the VRC performance [1-7].

* Corresponding author: Fateme Ahmadi Boyaghchi
Department of Mechanical Engineering, Faculty of Engineering & Technology, Alzahra University, Deh-Vanak, Tehran, Iran
Email: fahmadi@alzahra.ac.ir

Moreover, cycle modification utilizing a conventional ejector to recover some throttling process losses for raising the suction pressure of the compressor is a promising way for improving the performance of VRCs [8]. The conventional ejector enhanced VRC is named as the ejector-expansion refrigeration cycle (EERC). Several types of research can be found in the literature concerning EERCs to provide insight into many aspect of this improving method [7, 9-11].

Since EERC has a relatively low COP_{en}, many attempts have been carried out to develop advanced EERCs with higher COP_{en} [12]. For instance, Elakdhar et al. [13] presented a novel double-evaporator ejector refrigeration cycle for domestic application. The proposed system could operate at two different temperature levels through two expansion devices. A conventional gas to gas ejector was applied in this cycle to recover some throttling process losses. The performance of the system was evaluated using several refrigerants, such as R123, R124, R141b, R290, R153a, R717, R600a and R134a. The results showed that R141b gives the highest excellent performance and the cycle COP_{en} was improved up to 32% compared with the standard cycle.

Lawrence and Elbel [14] designed two double-evaporator refrigeration systems without a separator. Both systems were equipped with a conventional two-phase ejector and an evaporator before the compressor. It was found that the ejector enhanced cycle offered a COP_{en} improvement about 7% compared with standard double-evaporator refrigeration with expansion valves.

Elakhdar et al. [15] introduced a new double-evaporator refrigeration cycle, in which a conventional gas to gas ejector was placed between the separator and the compressor. A mixture of R290 and R600a as an environmentally friendly refrigerant in terms of lower GWP was used in this cycle. The mathematical simulation was developed to evaluate and compare the performances of the cycle with those of standard one. It was found that the COP_{en} of modified cycle was improved by 25.1% compared with the conventional double-evaporator refrigeration cycle proposed by Lin et al. [16].

Wang et al. [17] proposed a modified EERC using a conventional two-phase ejector in order to recover the expansion work. R600a was selected as an appropriate refrigerant in this cycle. They found that the modified EERC gives a higher pressure lift ratio and its COP_{en} reached about 1.1-6.2% higher than that of the conventional one.

Yu et al. [18] presented a two-stage ejector enhanced double-evaporator refrigeration cycle (TEDRC). In the proposed refrigeration cycle, an ejector with two suction inlets was applied to recover the throttling process losses. The performances of the cycle using refrigerant R32 were assessed theoretically and compared with

those of VRC and EERC. The results indicated that TEDRC yields better COP_{en} under the same operating conditions.

Zhou et al. [19] developed a novel dual-ejector enhanced dual-evaporator refrigeration cycle (DEDRC). In this cycle, two nozzles symmetrically placed could operate independently and had the advantage of a very efficient expansion work recovery. R600a and R134a were selected as refrigerants. The performance of DEDRC was investigated using mathematical simulation, and compared with that of EERC and VRC. The results showed a 6.94-8.93% COP_{en} improvement in comparison with EERC and VRC.

Kairouani et al. [20] presented a conventional ejector enhanced triple-evaporator refrigeration cycle (CETRC), in which two conventional two-phase ejectors were used to recover the compressor expansion work. The mathematical modeling of the ejector was carried out based on the constant-area flow model. R290, R600a, R717, R134a, R152a and R141b were used as the environment-friendly refrigerants. A comparative study between the novel cycle and conventional system with throttling valves was made. They found up to 80% improvement in the COP_{en} of CETRC compared with the conventional system.

In the present work, a new two-phase ejector enhanced triple-evaporator compression refrigeration cycle without separator operating with low GWP fluids (i.e., R717, R600a, R1234yf, and R290) is introduced for the first time. The proposed cycle is equipped with a dual-nozzle ejector which has the advantage of a more expansion loss recovery for improving the cycle COP_{en}. The performance of the proposed DETRC cycle is compared with that of the conventional ejector enhanced one (CETRC) under given operating conditions in order to represent the excellent energy-saving potential of the proposed cycle. Then, a mathematical modeling is performed to predict and compare the thermodynamic, economic and EI performances of the new cycle for selected refrigerants in detail. At the end, due to the same trends of economic and EI performances of DETRC, a bi-objective optimization based on the evolutionary algorithm is applied to maximize the exergetic performance and minimize the total product cost rate of the proposed cycle, simultaneously for each refrigerant in order to obtain the optimum solution points as Pareto frontier. Then, the

LINMAP decision making is used to ascertain the final optimum solution points from the various aspects.

Nomenclature

b	environmental impact per unit of exergy (Pts/kJ)
$\dot{B}$	environmental impact rate (Pts/s)
c	cost per unit of exergy ($/kJ)
$\dot{C}$	cost rate ($/s)
f_{env}	exergoenvironmental factor
f_{eco}	exergoeconomic factor
$\dot{Ex}$	total exergy flow rate (kW)
ex	specific exergy flow (kJ/kg)
h	specific enthalpy (kJ/kg)
i_r	Interest rate (%)
m	mass (kg)
$\dot{m}$	mass flow rate (kg/s)
N	system lifetime (year)
$\dot{Q}$	heat transfer rate (kW)
r_{Ejc}	ejector pressure lift ratio (-)
r_p	compressor pressure ratio (-)
s	specific entropy (kJ/kg K)
T	temperature ($^{\circ}$C)
U	velocity (m/s)
$\dot{W}$	compression power (kW)
Y	component-related environmental impact (Pts)
$\dot{Y}$	component-related environmental impact rate (Pts/s)
Z	cost associated with investment expenditures, ($)
$\dot{Z}$	cost rate associated with investment expenditures, ($/s)

Abbreviation

CETRC	Conventional ejector enhanced triple-evaporator refrigeration cycle
COP	Coefficient of performance
CRF	Capital recovery factor
DETRC	Dual-nozzle ejector enhanced triple-evaporator refrigeration cycle
DEDRC	Dual-ejector enhanced dual-evaporator refrigeration cycle
EI	Environmental impact
EERC	Ejector-expansion refrigeration cycle
GWP	Global warming potential
LCA	Life cycle assessment
NSGA-II	Non-dominated sorting genetic algorithm
ODP	Ozone depletion potential
SPECO	Specific exergy costing
TEDRC	Two-stage ejector enhanced double-evaporator refrigeration cycle
VRC	Vapour compression refrigeration cycle

Subscripts

0	reference environment state
1, 2, …	cycle states
Comp	compressor
CON	condenser
D	destruction
d	diffuse section
e	exit
Ejc	ejector
en	energy
Ev	evaporator
ex	exergy
F	fuel
i	inlet
is	isentropic process
k	kth component
L	loss
m	mixing section
n	nozzle section
P	product
Q	heat
tot	total
V	valve
W	power

Superscript

BF	pollutant formation
CI	capital investment

OM   operating and maintenance

Greek letters

η efficiency

μ entrainment ratio

φ mass flow rate allocation ratio

Φ maintenance factor

ω life cycle inventory associated with the production (Pts/kg)

2. Cycle description and assumptions

Figures 1.a and 1.b show a schematic diagram of the proposed refrigeration cycle and its P–h diagram. The proposed refrigeration cycle consists of a compressor, a condenser, three evaporators, a dual-nozzle ejector and two expansion valves.

The saturated vapor refrigerant enters the compressor (state 1) and is compressed to the high-side pressure (state 2). The hot refrigerant leaving the compressor flows through the condenser where it gets cooled (state 3) and obtains condensation by losing heat to the surroundings. Then, the condensate is spilled into two streams (states 4 and 9). One stream (state 9) enters evaporator 3 to cool evaporator 3

compartments after undergoing a pressure reduction in valve 1 (state 10) and the remaining stream is divided into two flows (states 5 and 6). One of them is throttled down to the intermediate pressure (state 7) and flows into evaporator 2 to produce cooling by drawing heat (state 8) and another stream is directly led to the first nozzle of the ejector (state 5). As shown in Fig. 1-c, a dual-nozzle ejector is composed of two nozzles (first and secondary nozzles), a suction chamber, a mixing chamber and a diffuser. Both the high-pressure saturated liquid partially from the condenser (state 5) and the middle-pressure saturated vapor coming from evaporator 2 (state 8) is used as the ejector primary flows. In the ejector, the motive streams are separately expanded to the low-pressure flows at the end of nozzles (states 5′ and 8′) and provide a suction region to entrain the saturated vapor from evaporator 3 (state 11). Then, the three streams mix in the mixing chamber and are compressed through the diffuser to evaporator 1 (state 12). The two-phase stream passing through evaporator 1 is evaporated (state 1) by taking heat from a cooling medium and finally is returned to the compressor to complete the cycle.

(a)

(b)
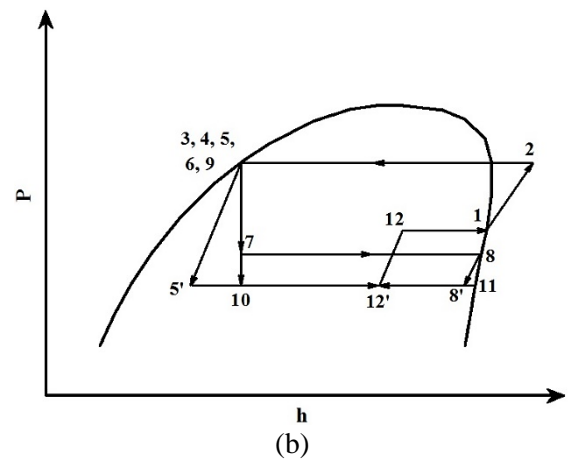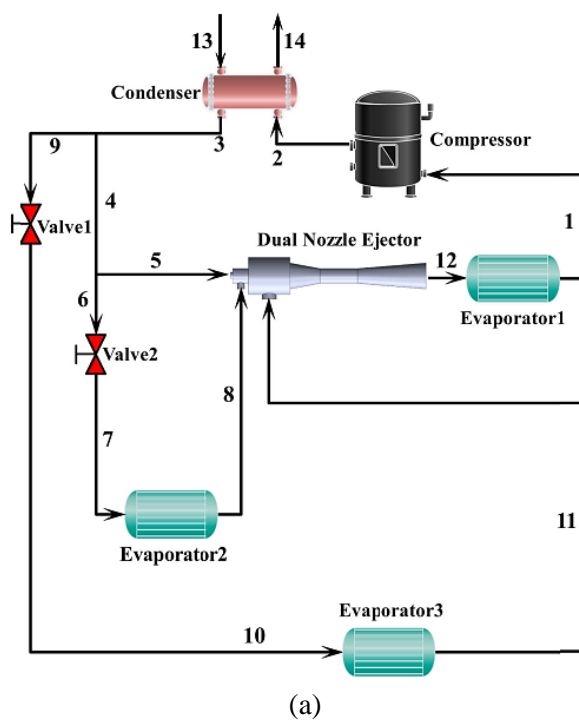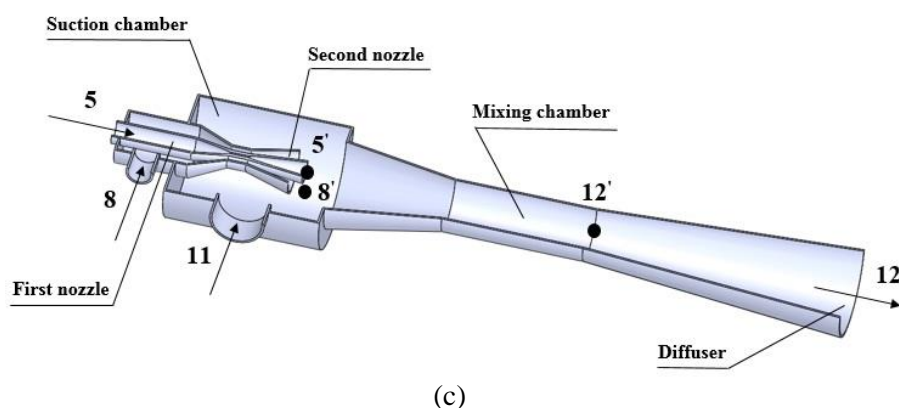
(c)

Fig. 1. (a) Proposed DETRC, (b) its P–h diagram and (c) configuration of the dual-nozzle ejector

To simplify the modeling of the proposed cycle, the following assumptions are made:

- The system components operate under the steady-state and steady-flow process;
- The heat and pressure losses in the various components are neglected;
- The throttling processes in expansion valves are isenthalpic;
- The refrigerant at the exit of evaporators and condenser is in a saturated state;
- The dual-nozzle ejector efficiencies are assumed as constant values (i.e., η_n=0.9, η_m=0.85 and η_d=0.8);
- The velocities of the primary and secondary fluids entering the dual-nozzle ejector are negligible.
- The ambient temperature and pressure are considered 25°C and 101.3 kPa, respectively.

3. Refrigerant selection:

In this work, R717, R600a, R1234yf and R290 are selected as candidate refrigerants in the proposed refrigeration cycle. Table 1 lists the properties and some environmentally-related parameters such as ozone depletion potential (ODP) and GWP of the selected refrigerants. The selected refrigerants belong to the special types, namely Natural and Hydrofluoroolefin (HFO) fluids [3, 21]. These refrigerants cannot destroy the ozone layer because they do not consist of chlorine. As can be seen, the GWPs of refrigerants are lower than 20 and the lowest one belongs to R717 (<1). Moreover, R1234yf with GWP value of 4 and zero ODP gives an excellent life cycle climate performance and has the least overall impact on the environments in refrigeration systems [22].

Table 1. Properties of selected refrigerants [3, 21].

Type	Natural			HFO
Refrigerant	R717	R290	R600a	R1234yf
Chemical formula	NH_3	C_3H_8	$(CH_3)_3CH$	CH_2CFCF_3
Molar mass (kg/kmol)	17.03	44.1	58.12	114.04
Critical temperature (°C)	132	97	135	94.70
Critical pressure (kPa)	11330	4300	3660	3382.20
NBP temperature[3] (°C)	-33	-42	-11.8	-29.49
ODP[1]	0	0	0	0
GWP[2]	<1	~20	~20	<4.4

[1]Ozone depletion potential;
[2]Global warming potential (for 100 years' integration);
[3]Normal boiling point.

4. Methodology

In this section, the energy and exergy-based analyses for the proposed refrigeration cycle are described. A computer program is developed via EES (Engineering Equations Solver) software to solve the resulting equations.

4.1. Energy Analysis

According to the assumptions made in section 2, the mass and energy balances of each component are detailed below.

Evaporator 1:

$$\dot{m}_1 = \dot{m}_2 \tag{1}$$

$$\dot{Q}_{Ev1} = \dot{m}_1 \left(h_1 - h_{12} \right) \tag{2}$$

Compressor:

$$\dot{m}_1 = \dot{m}_2 \tag{3}$$

$$\dot{W}_{Comp} = \dot{m}_1 \left(\frac{h_{2s} - h_1}{\eta_{is}} \right) \tag{4}$$

where η_{is} is the isentropic efficiency of the compressor given by [23]:

$$\eta_{is} = 0.85 - 0.046667 \left(r_P \right) \tag{5}$$

$r_P \left(= P_2/P_1 \right)$ refers to the pressure ratio of the compressor

Condenser:

$$\dot{m}_2 = \dot{m}_3 \tag{6}$$

$$\dot{Q}_{CON} = \dot{m}_2 \left(h_2 - h_3 \right) \tag{7}$$

Evaporator 2:

$$\dot{m}_7 = \dot{m}_8 \tag{8}$$

$$\dot{Q}_{Ev2} = \dot{m}_7 \left(h_8 - h_7 \right) \tag{9}$$

Evaporator 3:

$$\dot{m}_{10} = \dot{m}_{11} \tag{10}$$

$$\dot{Q}_{Ev3} = \dot{m}_{10} \left(h_{11} - h_{10} \right) \tag{11}$$

Valve 1:

$$\dot{m}_9 = \dot{m}_{10} \tag{12}$$

$$h_9 = h_{10} \tag{13}$$

Valve 2:

$$\dot{m}_6 = \dot{m}_7 \tag{14}$$

$$h_6 = h_7 \tag{15}$$

The mass and energy balances are also written for all branches.

Dual nozzle ejector:

The one-dimensional constant pressure mixing model is applied [24-26] to develop the mathematical model of the dual-nozzle ejector shown in Fig. 1-c. In this regard, the entrainment ratio (μ) which is a key parameter to simulate and assess the performance of the ejector is defined as [26]:

$$\mu = \frac{\dot{m}_{11}}{\dot{m}_5 + \dot{m}_8} \tag{16}$$

Here, $\dot{m}_{11}$ is the mass flow rate of secondary flow from evaporator 3. $\dot{m}_5$ and $\dot{m}_8$ are the mass flow rate of primary flows partially from the condenser and evaporator 2. Moreover, the mass flow allocation ratio for the primary streams is defined as:

$$\varphi = \frac{\dot{m}_8}{\dot{m}_5 + \dot{m}_8} \tag{17}$$

By applying the energy balance, the velocity of streams exiting two nozzles can be calculated as follows:

$$U_5 = \sqrt{2\eta_n \left(h_5 - h_{5,is} \right)} \tag{18}$$

$$U_8 = \sqrt{2\eta_n \left(h_8 - h_{8,is} \right)} \tag{19}$$

where η_n is the nozzle isentropic efficiency, h is enthalpy and index "is" refers to the isentropic process.

By using the energy balance for the mixing chamber, the velocity of the mixed stream can be expressed as:

$$U_m = \sqrt{\eta_m} \cdot \frac{\left(1 - \varphi \right) U_5 + \varphi U_8}{1 + \mu} \tag{20}$$

In Eq. (20), η_m is the mixing efficiency. Besides, the enthalpy of the mixed fluid can be calculated using the balance energy as follows:

$$h_m = \frac{\left(1 - \varphi \right) h_5 + \varphi h_8 + \mu h_{11}}{1 + \mu} - \frac{U_m^2}{2} \tag{21}$$

The enthalpy of the stream exiting the diffuser can be calculated using the definition of the diffuser efficiency (η_d) as follows:

$$h_{12} = h_m + \frac{(h_{12,is} - h_m)}{\eta_d} \tag{22}$$

The velocity of the mixed stream at the exit of the diffuser can be obtained using the energy balance:

$$U_{12} = \sqrt{U_m^2 - 2(h_{12} - h_m)} \tag{23}$$

The COP$_{en}$ for the analyzed system is defined as:

$$COP_{en} = \frac{\dot{Q}_{Ev}}{\dot{W}_{Comp}} \tag{24}$$

In Eq. (24), $\dot{Q}_{Ev}$ refers to the sum of the cooling loads produced via evaporators.

4.2. Exergy-based analyses

Unlike the energy analysis, exergy analysis is a convenient tool to identify the type and magnitude of thermodynamic irreversibilities and the exergy loss due to the exergy transfer to the environment within each component of the energy system. The exergy balance equation for a control volume can be described as follows [27]:

$$\dot{Ex}_D = \sum_i \dot{Ex}_i - \sum_e \dot{Ex}_e + \dot{Ex}_Q - \dot{Ex}_W \tag{25}$$

Here, $\dot{Ex}_D$ is the total exergy destruction. $\dot{Ex}_Q$ is the exergy flow related to the heat transfer through the control volume boundaries and is given by:

$$\dot{Ex}_Q = \dot{Q}\left(1 - \frac{T_0}{T}\right) \tag{26}$$

$\dot{Ex}_w$ is the exergy rate associated with the work which is calculated as follows:

$$\dot{Ex}_W = \dot{W} \tag{27}$$

In Eq. (25), $\dot{Ex}_i$ and $\dot{Ex}_e$ are related to the exergies of inlet and outlet streams of matter and are defined by:

$$\dot{Ex} = \dot{m}.ex \tag{28}$$

where *ex* is the physical exergy described as:

$$ex = (h - h_0) - T_0(s - s_0) \tag{29}$$

Eq. (29) can be categorized as fuel, product and loss exergies for each component. The definition of fuel, product and loss exergy flows for each component of the desired cycle are summarized in Table 2.

The exergetic coefficient of performance (COPex) for the cycle can be calculated using Eq. (30):

$$COP_{ex} = \frac{Q_{Ev1}\left(1 - \frac{T_0}{T_{Ev1}}\right) + Q_{Ev2}\left(1 - \frac{T_0}{T_{Ev2}}\right) + Q_{Ev3}\left(1 - \frac{T_0}{T_{Ev3}}\right)}{\dot{W}_{Comp}} \tag{30}$$

Exergoeconomic analysis is applied to calculate the cost per unit exergy of the streams in an energy system. In this work, the specific exergy costing (SPECO) approach is adopted because of its straightforward scheme and efficient calculation [28]. The cost balance equation for each component is defined as [27]:

Table 2. Definition of fuel, product, and loss exergy flow rates of the refrigeration cycle components

Component	Fuel	Product	Loss
Compressor	$\dot{Ex}_W$	$\dot{Ex}_2 - \dot{Ex}_1$	-
Condenser	$\dot{Ex}_2 - \dot{Ex}_3$	-	$\dot{Ex}_{14} - \dot{Ex}_{13}$
Ejector	$\dot{Ex}_5 + \dot{Ex}_8 + \dot{Ex}_{11}$	$\dot{Ex}_{12}$	-
Evaporator 1	$\dot{Ex}_{12} - \dot{Ex}_1$	$\dot{Ex}_{Q,Ev1}$	-
Evaporator 2	$\dot{Ex}_7 - \dot{Ex}_8$	$\dot{Ex}_{Q,Ev2}$	-
Evaporator 3	$\dot{Ex}_{10} - \dot{Ex}_{11}$	$\dot{Ex}_{Q,Ev3}$	-

$$\dot{C}_Q + \sum_i \dot{C}_i + \dot{Z} = \sum_e \dot{C}_e + \dot{C}_W \qquad (31)$$

where $\dot{C}_Q$ and $\dot{C}_W$ are the cost rates associated with heat transfer and work and can be calculated as follows:

$$\dot{C}_Q = c_Q.\dot{Ex}_Q \qquad (32)$$

$$\dot{C}_W = c_W.\dot{Ex}_W \qquad (33)$$

Here $\dot{C}_i$ and $\dot{C}_e$ are the cost rates related to entering and exiting streams of matter:

$$\dot{C} = c.\dot{Ex} \qquad (34)$$

In Eqs. (32) to (34), c denotes the average cost per unit of exergy. The $\dot{Z}$ appeared in Eq. (31), is the total cost rate of investment expenditures which is the sum of the cost rates associated with capital investment ($\dot{Z}^{CI}$) and operating and maintenance ($\dot{Z}^{OM}$). The value of $\dot{Z}$ is calculated as:

$$\dot{Z} = \frac{Z \times \Phi \times CRF}{N} \qquad (35)$$

Here, Z is the purchase cost of each component expressed in [29, 30], Φ is the maintenance factor (i.e. 1.06) and CRF refers to the capital recovery factor being expressed by [27]:

$$CRF = \frac{i_r(1+i_r)^N}{(1+i_r)^N - 1} \qquad (36)$$

In Eq. (36), i_r is the interest rate (i.e. 10%) and N refers to the system life (i.e. 20 years and 7446 working hours per year at full capacity).

The cost balance and cost rates per unit of exergy are calculated using additional auxiliary equation listed in Table 3 based on Fuel-Product rules.

The total product cost rate of the system is the sum of the cooling loads cost produced in evaporators as follows:

$$\dot{C}_{P,tot} = c_{Ev1}\dot{Ex}_{Q,Ev1} + c_{Ev2}\dot{Ex}_{Q,Ev2} + c_{Ev3}\dot{Ex}_{Q,Ev3} \qquad (37)$$

The cost rate associated with exergy destruction ($\dot{C}_D$) and exergoeconomic factor (feco) are two major parameters which play important roles in exergoeconomic analysis. These criteria can be defined as follows:

$$\dot{C}_D = c_F.\dot{Ex}_D \qquad (38)$$

Here, c_F is the average cost per unit of fuel exergy.

$$f_{eco} = \frac{\dot{Z}}{\dot{Z} + \dot{C}_D} \qquad (39)$$

The total exergy destruction cost rate ($\dot{C}_{D,tot}$) and total exergoeconomic factor ($f_{eco,tot}$) are defined as follows:

$$\dot{C}_{D,tot} = \sum_k \dot{C}_{D,k} \qquad (40)$$

$$f_{eco,tot} = \frac{\dot{Z}_{tot}}{\dot{Z}_{tot} + \dot{C}_{D,tot}} \qquad (41)$$

Exergoenvironmental analysis is a combination of the exergy concept and life cycle assessment (LCA) which is used to have a better understanding of the performance of the proposed cycle from the EI aspect. LCA is applied to evaluate the EI related to a component (Y) over its lifetime and it is assessed here using ECO-indicator'99 [31].

Table 3. Cost balance and auxiliary equations for components of the proposed cycle

Component	Cost balance	Auxiliary equation
Compressor	$c_1\dot{Ex}_1 + c_W\dot{Ex}_W + \dot{Z}_{Comp} = c_2\dot{Ex}_2$	$c_W = 0.33$ \$/kWh (known)
Condenser	$c_2\dot{Ex}_2 + c_{13}\dot{Ex}_{13} + \dot{Z}_{Con} = c_3\dot{Ex}_3 + c_{14}\dot{Ex}_{14}$	$c_2 = c_3$ (Fuel rule)
Ejector	$c_5\dot{Ex}_5 + c_8\dot{Ex}_8 + c_{11}\dot{Ex}_{11} + \dot{Z}_{Ejc} = c_{12}\dot{Ex}_{12}$	-
Evaporator 1	$c_{12}\dot{Ex}_{12} + c_{Q,Ev1}\dot{Ex}_{Q,Ev1} + \dot{Z}_{Ev1} = c_1\dot{Ex}_1$	$c_{12} = c_1$ (Fuel rule)
Evaporator 2	$c_7\dot{Ex}_7 + c_{Q,Ev2}\dot{Ex}_{Q,Ev2} + \dot{Z}_{Ev2} = c_8\dot{Ex}_8$	$c_7 = c_8$ (Fuel rule)
Evaporator 3	$c_{10}\dot{Ex}_{10} + c_{Q,Ev3}\dot{Ex}_{Q,Ev3} + \dot{Z}_{Ev3} = c_{11}\dot{Ex}_{11}$	$c_{10} = c_{11}$ (Fuel rule)
Valve 1	$c_9\dot{Ex}_9 + \dot{Z}_{V1} = c_{10}\dot{Ex}_{10}$	-
Valve 2	$c_6\dot{Ex}_6 + \dot{Z}_{V2} = c_7\dot{Ex}_7$	-

The amount of Y for each device of energy system can be calculated using Eq. (42):

$$Y = \sum m.\omega \qquad (42)$$

Here, m is the mass of constituent materials of each component and ω is the life cycle inventory associated with the production which can be obtained from LCA and ECO-indicator' 99 [30, 32].

Meanwhile, the average EI per exergy unit (b) associated with the production of each stream can be calculated by applying the environmental balance for a component and auxiliary equations based on the Product and Fuel rules. The exergoenvironmental balance for a component is formulated by:

$$\dot{B}_Q + \sum_i \dot{B}_i + \left(\dot{Y} + \dot{B}^{PF}\right) = \sum_e \dot{B}_e + \dot{B}_W \qquad (43)$$

Here, $\dot{B}(= b\dot{E}x)$ is EI rate associated with exergy flow. The EI rates associated with heat and work transfers are calculated as follows:

$$\dot{B}_Q = b \cdot \dot{E}x_Q \qquad (44)$$

$$\dot{B}_W = b \cdot \dot{W}$$

The subscripts "i" and "e" refer to entering and exiting streams. $\dot{Y}(= Y/N)$ is the component- related EI rate. $\dot{B}^{PF}$ is the EI of pollutant formation within the component and it is considered only when a chemical reaction takes place; otherwise, it is zero.

The total product EI rate of the system is defined as follows:

$$\dot{B}_{P,tot} = b_{Ev1}\dot{E}x_{Q,Ev1} + b_{Ev2}\dot{E}x_{Q,Ev2} + b_{Ev3}\dot{E}x_{Q,Ev3} \qquad (45)$$

Similarly, the EI related to the exergy destruction $(\dot{B}_D)$ and exergoenvironmental factor (f_{env}) are defined to assess the EI performance of the cycle as follows:

$$\dot{B}_D = b_F.\dot{E}x_D \qquad (46)$$

Here, c_F is the average cost per unit of fuel exergy.

$$f_{env} = \frac{\dot{Y}}{\dot{Y} + \dot{B}_D} \qquad (47)$$

The total exergy destruction EI rate $(\dot{B}_{D,tot})$ and total exergoenvironmental factor $(f_{env,tot})$ are defined as follows:

$$\dot{B}_{D,tot} = \sum_k \dot{B}_{D,k} \qquad (48)$$

$$f_{env,tot} = \frac{\dot{Y}_{tot}}{\dot{Y}_{tot} + \dot{B}_{D,tot}} \qquad (49)$$

4.3. Multi-objective optimization and decision making

Multi-objective optimization is applied when an energy system confronts several conflicting objectives. Based upon this, as one objective improves, another deteriorates. Therefore, there does not exit a single optimum solution that is the best with respect to all objectives. Instead, through the optimization, a set of optimal solutions, called as Pareto optimal solutions, is obtained and the corresponding objective function values are called the Pareto frontier. [33, 34]. A Pareto front in the space of objectives refers to a set of solutions that are non-dominated by other solutions but are superior to the rest of the solutions in the search space [35]. The Pareto frontier is bounded by an ideal solution and a non-ideal solution which specify respectively the upper and lower bounds of objective functions in Pareto optimal solutions [36].

In this investigation, Pareto frontier is achieved using an evolutionary algorithm based on elitist non-dominated sorting genetic algorithm (NSGA-II) proposed by Deb [33]. The detailed procedure adopted by NSGA-II can be found in Ref. [34].

In multi-objective problems, the decision making is required to select the final optimal solution from the Pareto frontier. In this study, one of the most recognized decision making called LINMAP method is used. In this method, the solution with minimum distance from the ideal solution is selected as a final optimal solution [37].

5. Results and discussion:

In the first step, a comparison of operating conditions and performance ranges for the novel DETRC, and CETRC proposed by [20] is carried out in order to show the advantage of the present work.

The simulation of DETRC and CETRC are performed at the following operating conditions: $T_{CON}=45^{o}C$, $T_{Ev1}=5^{o}C$, $T_{Ev2}=-18^{o}C$, $T_{Ev3}=-28^{o}C$ and R141b as refrigerant [20]. The

amounts of COP_{en} for DETRC and CETRC are obtained about 3.37 and 2.71, respectively which shows that the present cycle has a 24.35% higher COP_{en} than that of CETRC. On the other hand, CETRC improves COP_{en} up to 80% as compared with the conventional multi-evaporator refrigeration system using throttling valves [12]. The COP_{en} improvement of DETRC is because of the fact that in this layout the major portion of refrigerant leaving the condenser acts as the dual-nozzle ejector primary flows with higher enthalpy. Based upon this, the ejector pressure lift ratio is considerably higher which causes the COP_{en} of DETRC to increase. In dead, COP_{en} improvement occurs when the expansion work recovery is performed. Therefore, using a dual-nozzle ejector can reduce the large throttling losses in the refrigeration cycle.

Table 4 summarizes the comparisons of the COP_{en} variations with varying evaporating and condensing temperatures for both cycles. It is obvious that the performance of DETRC is significantly affected by system operating conditions. It can be found that the DETRC gives better performance at lower T_{Ev2}, T_{Ev3} and T_{CON} and higher T_{Ev1} due to the large enthalpy of streams entering ejector as the primary flows. In these cases, the expansion ratio of the dual-nozzle ejector increases and then more expansion losses in DETRC can be recovered.

In the following simulation, the effect of evaporating temperatures, condensing temperature and ejector allocation ratio on the thermodynamic, economic and EI performances of DETRC are evaluated and compared for each selected refrigerant. Meanwhile, the influence of the evaporating temperatures on the total exergoeconomic and exergoenvironmental factors of the proposed cycle is assessed.

Figure 2-a shows the effect of T_{Ev1} on Q_{Ev}, r_{Ejc} and COP_{en} of the cycle, where the evaporating temperatures in evaporators 2 and 3 are fixed at -20°C and -30°C, respectively and the allocation ratio is set at 0.5. As T_{Ev1} ranges from -5°C to 5°C, the entrainment ratio remains constant while the ejector pressure lift ratio (P_{12}/P_{11}) and the available expansion ratio (P_5/P_{11}) increase due to the larger exit pressure of the ejector. Hence, more expansion losses can be recovered in the cycle and the corresponding compressor consumed power reduces, significantly. The increase of T_{Ev1} does not affect the cooling loads in evaporators 2 and 3 and it has a slight negative influence on evaporator 1 due to the growth of the stream enthalpy at the exit of the ejector. It can be seen that R717 refrigerant gives the uppermost values of Q_{Ev} and COP_{en} over the whole range of T_{Ev1} because under a given condition, the value of R717 enthalpy is higher than that of other studied refrigerants. Therefore, the ranges of Q_{Ev} and power vary from 959.2 kW to 221.1 kW and 334.2 kW to 221.1 kW, respectively which improve COP_{en} by 2.87-4.19 (nearly 46% increment).

Figure 2-b depicts the variations of thermal performances of the proposed cycle with TEv2. For a fixed condensing temperature, when TEv2 ranges from -28oC to -10oC, the enthalpy of the mixed stream inside the ejector mixing section decreases and consequently the enthalpy at the ejector exit reduces, while other parameters remain almost constant. Hence, only the amounts of cooling loads produced in evaporators 2 and 1 increase. Since the compressor consumed power does not vary with TEv2, the same improvement trend is observed for COPen.

Table 4. Comparison of simulation results for the present cycle and CETRC at standard operating conditions for R141b

COP$_{en}$ ranges of	Operating conditions			
	$T_{CON} = 30 - 45°C$	$T_{Ev1} = -5$ to $10°C$	$T_{Ev2} = -20$ to $-10°C$	$T_{Ev3} = -30$ to $-25°C$
CETRC [20]	$4.12 - 2.71$	$2.13 - 2.94$	$2.60 - 2.74$	$2.60 - 2.69$
DETRC	$6.56 - 3.37$	$2.13 - 4.15$	$3.36 - 3.41$	$3.34 - 3.42$
Improved COP$_{en}$	$59.22 - 24.35\%$ [a]	$0 - 40.13\%$ [a]	$29.23 - 24.45\%$ [a]	$28.46 - 27.13\%$ [a]

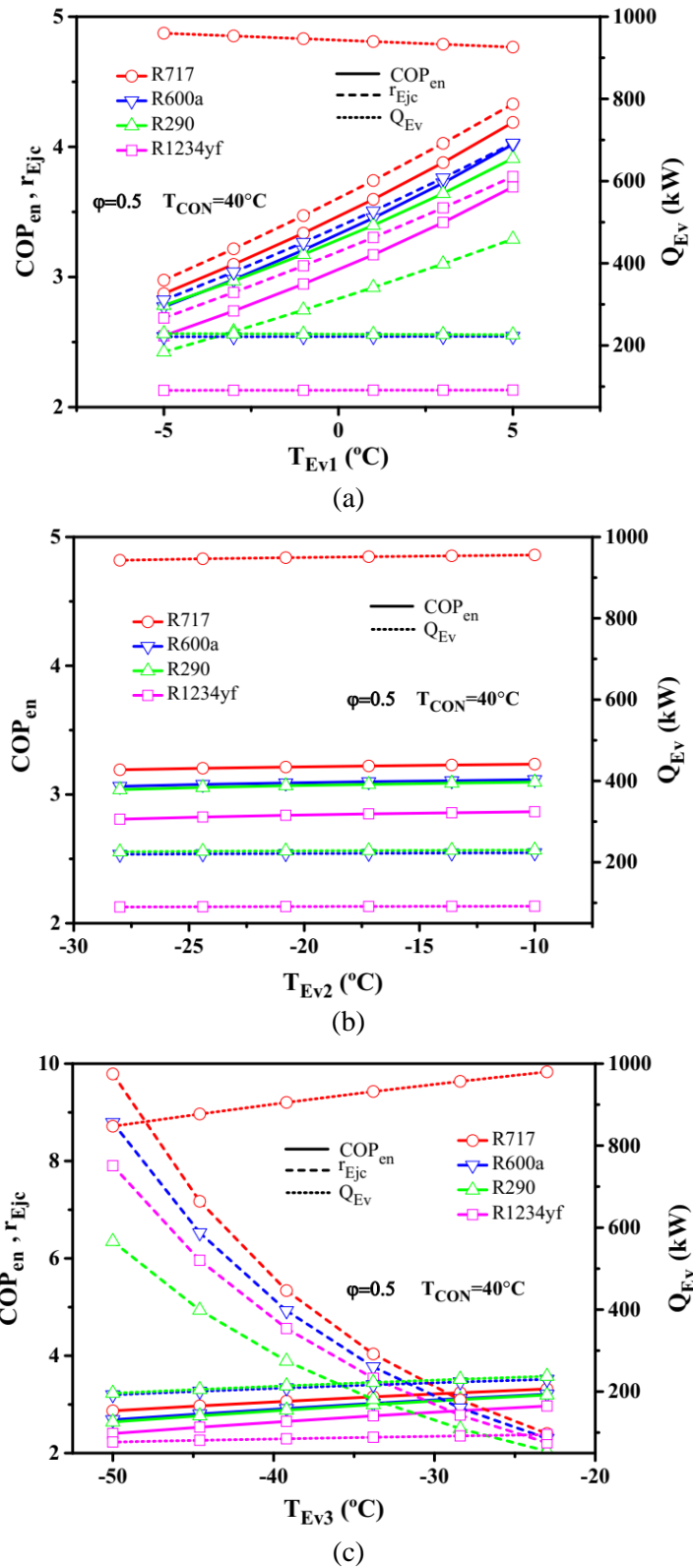[a] Compare to the CETRC in [20].

(a)

(b)

(c)

Fig. 2 The effect of the evaporating temperatures on the Q_{Ev} and COP_{en}

Outcomes indicate that COP_{en} and Q_{Ev} can be increased by 3.2-3.24 and 942.7kW-955.8kW, respectively and the highest increment in COP_{en} of the cycle is obtained by about 2.1% for R1234yf.

The effect of evaporating temperature, T_{Ev3}, on Q_{Ev}, r_{Ejc} and COP_{en} is shown in Fig. 2-c. For the given conditions, with increasing T_{Ev3}, the secondary flow pressure and its enthalpy increase which result in a drastic reduction in the pressure lift ratio of the ejector. Thus, the cooling load produced in evaporator 3 increases. Any increase in the enthalpy increases the mixed stream enthalpy inside the ejector mixing chamber and reduces the ejector exit stream enthalpy. Thus, the heat transfer rate of evaporator 1 grows. As explained earlier, R717 produces higher Q_{Ev} and due to the higher compressor consumed power in relation to other studied refrigerants, its COP_{en} increases from 2.87 to 3.32. The maximum increments in COP_{en} and Q_{Ev} are 23.5% for R1234yf followed by R290 with a value of 21%.

Figure 3 shows the COP_{en}, Q_{Ev} and r_P values versus the condensing temperature at the following operating condition: T_{Ev1}=-2°C, T_{Ev2}=-20°C and T_{Ev3}=-30°C. It can be seen that the ejector available expansion ratio and corresponding pressure are found to increase with varying the condensing temperature from 30°C to 50°C and, hence the heat transfer

rates in all evaporators drop due to the increments in entrance streams enthalpies. Moreover, with increasing the condensing temperature the pressure ratio of the compressor increases rapidly which results in an increment in consumed power of the cycle. Therefore, the COP_{en} of the cycle will reduce. The results show that more than 50% reduction can be obtained for COP_{en} for all refrigerants and the lowest decrement in Q_{Ev} is obtained by 9.93% for R717.

Figure 4 shows the influence of the mass flow allocation ratio on the energetic performances of the cycle. At the special operating conditions, the variation of φ from 0.4 to 0.68 affects the refrigeration capacity of the evaporators due to the reduction of the ejector entrainment ratio from 0.73 to 0.2. It can be seen that the heat transfer rate in evaporators 1 and 2 increases, whereas variation tendency of the refrigeration load in evaporator 3 is opposite due to the constant mass flow rate. On the other hand, the required power does not vary due to the nearly constant pressure ratio. From these results, the value of COP_{en} increases slightly with increasing φ. For all refrigerants, the COP_{en} and Q_{Ev} improvements are nearly 0.1 and 28kW.

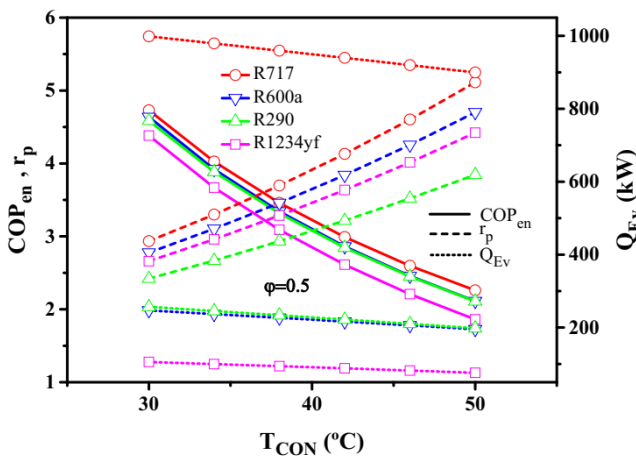The COPex, $\dot{C}_{p,tot}$ and $\dot{B}_{p,tot}$ variations with evaporating temperatures are delineated

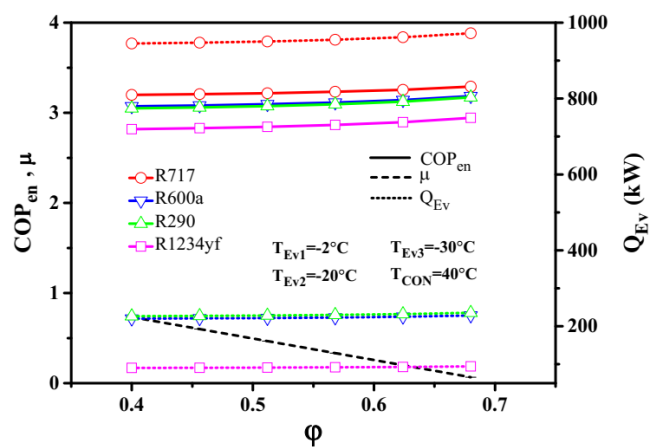**Fig. 3.** The effect of condensing temperature on the Q_{Ev} and COP_{en}

Fig. 4 The effect of mass flow allocation ratio on the QEv and COPen

in Figs. 5-a to c. Referring to Fig. 2-a, the same variations trend can be observed for COP_{en} and COP_{ex}. Based on Fig. 5-a, increasing T_{Ev1} increases COP_{ex} due to the reductions of the compressor consumed power and total exergy destruction for all refrigerants. The highest reduction in the total exergy destruction is obtained about 63.6 kW (i.e., 21.64%-14.97% reduction in exergy destruction ratio) for R717 which leads to a 1.45 times increment in COP_{ex}. According to the results, the major contribution of the total exergy destruction is directly related to the compressor. Hence, any reduction in the compressor required power affects the total exergy destruction of the cycle, positively. As it is well known, the cost and EI rates performances of the cycle are considerably governed by the change of T_{Ev1}. Due to the reduction of total exergy destruction rate, the total cost and EI rates associated with exergy destruction rate also reduce which lead to the decrements in product cost and EI rates of the overall cycle. In addition, exergy unit of product cost and EI of all evaporators drops. These improvements are relatively large for R717 (i.e., 20.4 $/h and 1.67 Pts/h) owing to its relatively high thermodynamic properties at the same conditions. It can be seen that R1234yf gives the lowest cost and EI performances by 9.1-6.33 $/h and 0.74-0.51 Pts/h, respectively with varying T_{Ev1}.

According to Fig. 5-b, increasing T_{Ev2} has a slightly negative influence on the COP_{ex} for all refrigerants. This is because of the fact that with varying T_{Ev2}, the total exergy destruction rate of the cycle increases due to the high increment in the ejector exergy destruction rate, and consequently the exergy associated with heat transfer inside evaporator 2 drops considerably. The lowest reduction of COP_{ex} is 0.52-0.46 (11.65%) for R1234yf while the maximum reduction is 13.3% for R717 that has the highest range of COP_{ex} (i.e., 0.62-0.54). Slight reduction trends are observed for the product cost and EI rates of the overall cycle when T_{Ev2} increases. It can be seen that as T_{Ev2} varies, the product cost and EI rate of the cycle improve by 3.4 $/h and 0.28 Pts/h for R717 that causes the maximum reductions in the cost and EI performances of the cycle.

Whereas, the cycle has the lowest cost and EI performances by 8.34-8.01 $/h and 0.67-0.65 Pts/h for R1234yf.

Figure 5-c displays the variation of exergy-based performances of the cycle with T_{Ev3} at the given operating conditions. When T_{Ev3} increases the exergy destruction rates of the ejector and evaporator 1 are found to increase while it may reduce inside evaporator 3. These effects increase the total exergy destruction of the overall cycle for all refrigerants and thus the COP_{ex} reduces. The highest reduction of COP_{ex} is 21% for R717 ranging from 0.69-0.54 and the minimum reduction is obtained 10.8% for R1234yf which has the lowest range of COP_{ex}. On the other hand, T_{Ev3} varying reduces the total product cost and EI rates of the cycle due to the reduction of product cost and EI rates of evaporator 3. It can be seen that R717 gives the maximum cost and EI performances owing to the higher thermodynamic properties among the other refrigerants while R1234yf gives better product cost and EI rates by 9.1-7.98 $/h and 0.74-0.65 Ptsh, respectively.

Figure 6 displays the COP_{ex}, $\dot{C}_{p,tot}$ and $\dot{B}_{p,tot}$ values versus the condensing temperature when T_{Ev1}=-2°C, T_{Ev2}=-20°C and T_{Ev3}=-30°C. As expected, with an increase of T_{CON} from 30°C to 50°C, a strong reduction trend for COP_{ex} is obtained due to the reduction of the cooling load produced in evaporators and increase of compressor consumed power. The exergetic performance of the cycle drops 57.49%, 54.38%, 53.77% and 52.02% for R1234yf, R600a, R290 and R717, respectively. On the other hand, with increase of T_{CON}, the total exergy destruction cost and EI rates increase in which the condenser has the highest contribution. Moreover, the cost and EI exergy unit of the evaporators increase. These reasons lead to the weakening of cost and EI performances of the cycle. As can be seen, the minimum ranges of product cost and EI rates belong to R1234yf by 7.27-9.15 $/h and 0.59-0.74 Pts/h and R290 gives the lowest reductions in cost and EI performances by 19.75% and 19.93%, respectively.
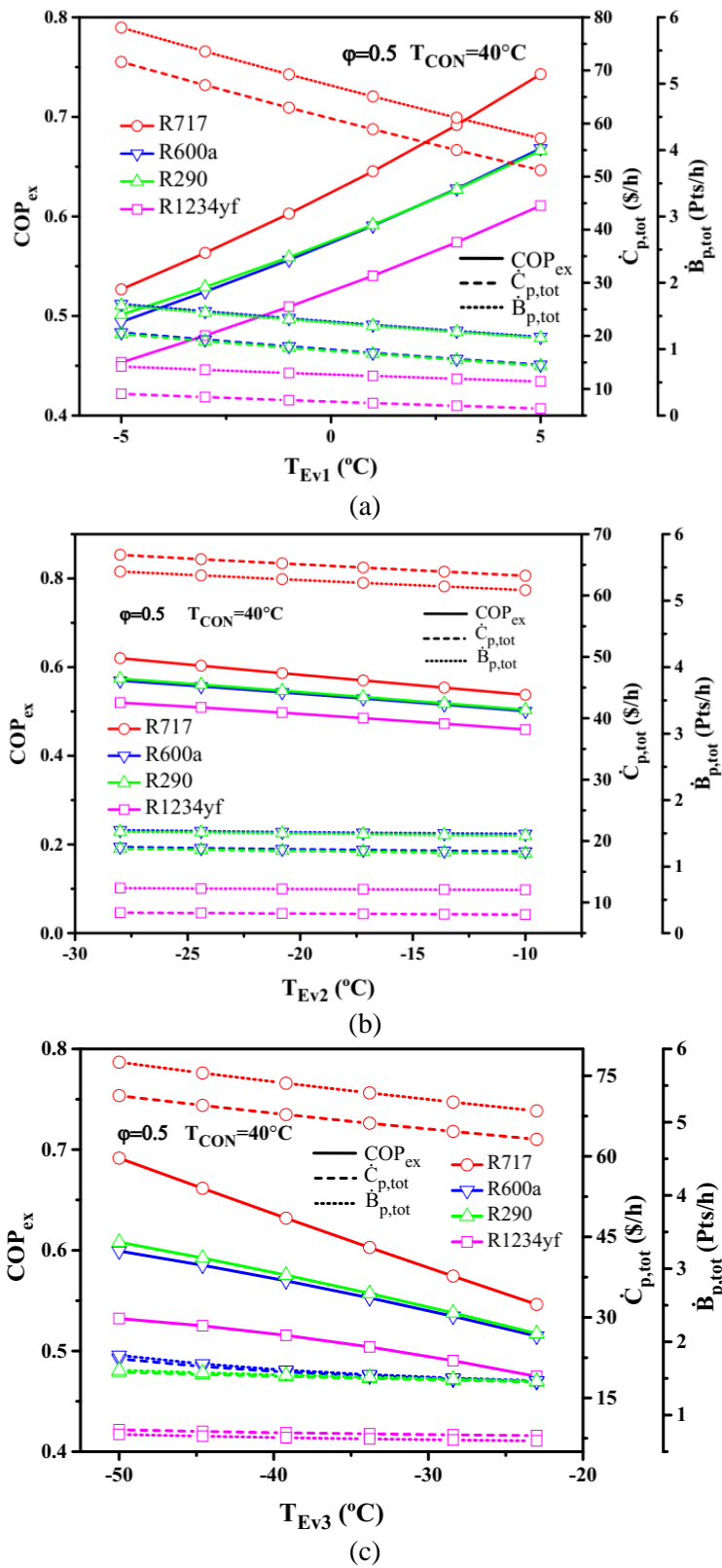
(a)

(b)

(c)

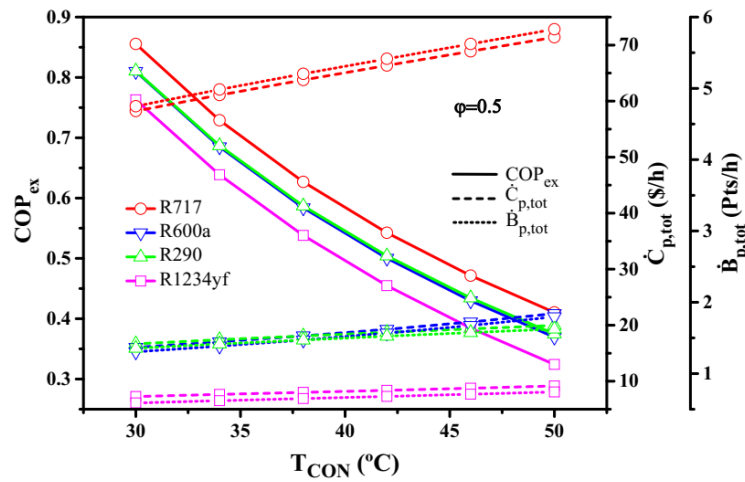**Fig. 5** The effect of evaporating temperaturs on the exergy-based criteria

Fig. 6 The effect of condensing temperatur on the exergy-based criteria

Figure 7 indicates the variations of φ with mass allocation ratio. With increasing φ the total exergy destruction is found to increase in which evaporator 1 contributes major exergy destruction rate. Moreover, the product exergy of evaporator 3 reduces. These reasons cause a reduction in COP_{ex}. As can be seen, the highest range of cycle COP_{ex} reduces by 0.59-0.53 (8.84% reduction) for R717 and the lowest reduction of COP_{ex} is 6.34% for R1234yf. Moreover, φ variation causes the product cost and EI rates of the system to reduce due to the reductions of exergy unit of cost and EI of all evaporators. Based upon this, the cost and EI performances of the system are improved by 3.91%, 3.96%, 3.29% and 3.06% for R717, R600a, R1234yf

and R290, respectively. It can be seen that R1234yf gives the best cost and EI performances with ranges of 8.20-7.93 \$/h and 0.66-0.64 Pts/h.

Figures 8-a to c illustrate the variations of the total exergoeconomic and exergoenvironmental factors, $f_{eco,tot}$ and $f_{env,tot}$, with evaporating temperatures. It can be seen that for a considerable range of evaporating temperatures, the values of $f_{eco,tot}$ and $f_{env,tot}$ are obtained lower than 9% and 2%, respectively, which represent that exergy destruction cost and EI rates of overall cycle strongly affect the economic and environmental performances of the cycle. These criteria can be improved by replacing the cycle components with more effective ones.
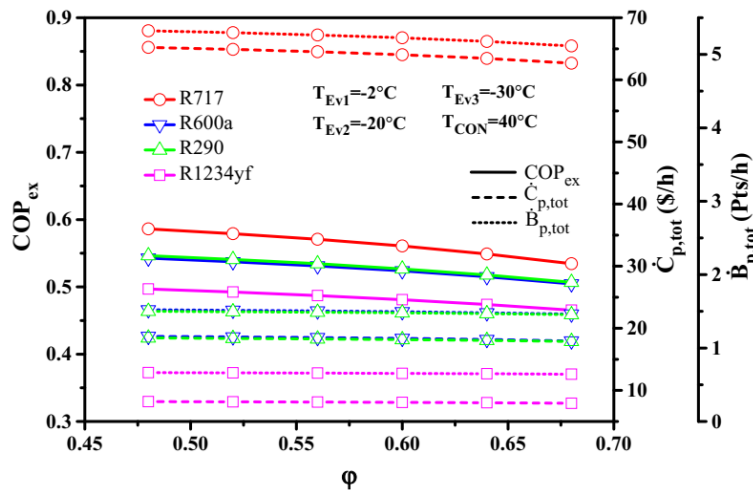

Fig. 7 The effect of mass flow allocation ratio on the exergy-based criteria
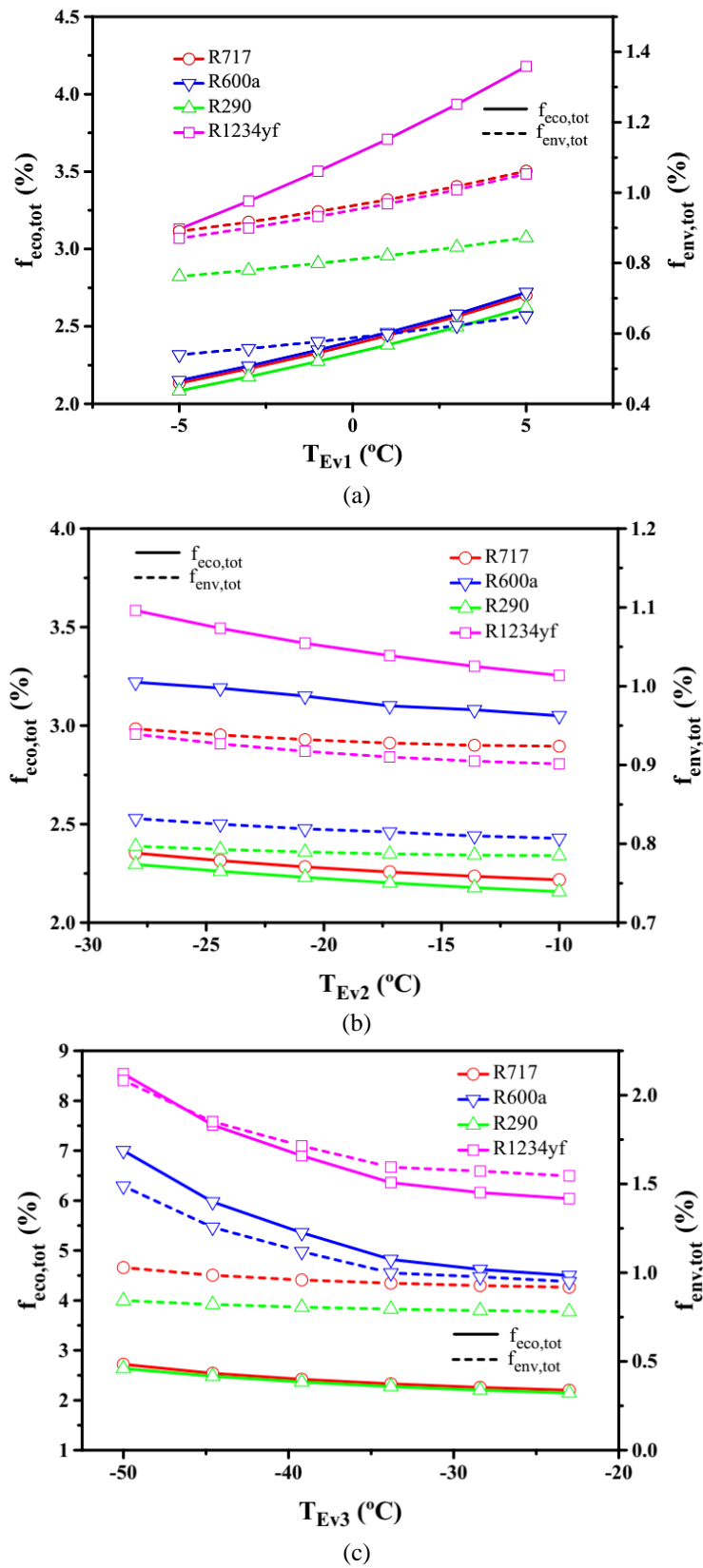
(a)

(b)

(c)

Fig. 8. The Effect of evaporating temperatures on the exergoeconomic and exergoenvironmental factors.

5.1. Optimization results

According to the results discussed in section 5, the total cost and EI rates of the cycle represent the same trend with variations of design parameters. Therefore, bi-objective NSGA-II optimization is conducted to maximize COP_{ex} (Eq. (30)) and minimize $\dot{C}_{p,tot}$ (Eq. (37)) of the proposed refrigeration cycle. In this regard, the six design parameters with corresponding constraints listed in Table 5 are considered as decision variables. Meanwhile, tuning parameters of the genetic algorithm used for convergence of the results are listed in Table 6.

The Pareto front curves with bi-objective COP_{ex} and $\dot{C}_{p,tot}$ for four studied refrigerants are obtained and shown in Figs. 9-a to d. All points existing in the Pareto front are non-dominated and be selected as a final solution by applying the decision-maker. According to Figs. 9-a to d, a trade-off trend between exergetic and economic performances of the cycle can be observed so that with an increase of COP_{ex}, $\dot{C}_{p,tot}$ can rise strongly. As can be seen, the ideal point at which both objectives have the best values does not exist on the Pareto frontier. Therefore, the closest point of the Pareto frontier to the ideal point obtained by LINMAP procedure is considered as a final optimum solution. Points A and B represent the highest and the lowest values of COP_{ex} and $\dot{C}_{p,tot}$, respectively on the Pareto frontier. Table 7 presents the detailed parameters with corresponding optimal ranges for all studied refrigerants. Moreover, to provide a convenient relation for the optimal design of the cycle, a curve is fitted to the optimum points existing on Pareto frontier with the following equations for each refrigerant:

$$\dot{C}_{P,tot} = 37.44 \times COP_{ex}^3 - 76.74 \times COP_{ex}^2 + 46.541 \times COP_{ex} + 8.3833$$
$$(0.712 \leq COP_{ex} \leq 1.683 \text{ for R717})$$

$$\dot{C}_{P,tot} = 28.826 \times COP_{ex}^3 - 62.492 \times COP_{ex}^2 + 47.559 \times COP_{ex} - 6.2526$$
$$(0.702 \leq COP_{ex} \leq 1.495 \text{ for R600a})$$

$$\dot{C}_{P,tot} = 26.68 \times COP_{ex}^3 - 56.929 \times COP_{ex}^2 + 42.144 \times COP_{ex} - 3.9773$$
$$(0.668 \leq COP_{ex} \leq 1.538 \text{ for R290})$$

$$\dot{C}_{P,tot} = -5.873 \times COP_{ex}^3 + 29.562 COP_{ex}^2 - 33.856 \times COP_{ex} + 14.075$$
$$(0.653 \leq COP_{ex} \leq 1.17 \text{ for R1234yf})$$

Table 5. Decision variables and their reasonable ranges

Parameter	Lower range	Upper range
T_{Ev1} (°C)	-5	5
T_{Ev2} (°C)	-28	-10
T_{Ev3} (°C)	-50	-23
T_{CON} (°C)	30	50
φ	0.48	0.68
$\dot{m}$ (kg/s)	0.6	2

Table 6. Genetic algorithm parameters

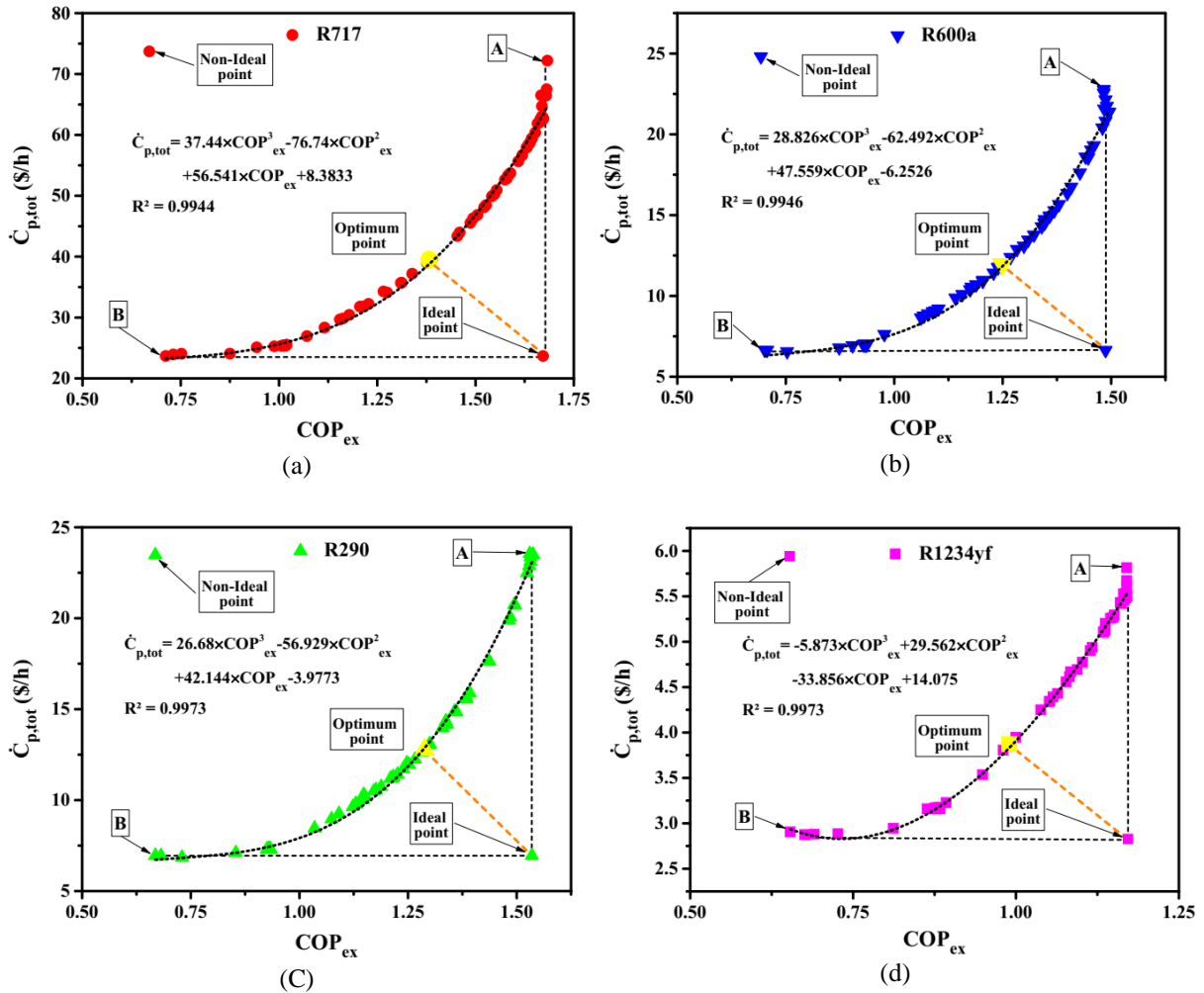| Parameter	Value
Population size	200
Generation size	100
Crossover fraction	0.8
Mutation rate	0.01
Selection process	Tournament

Fig. 9. The Pareto frontier optimal distribution for COP_{ex} and $\dot{C}_{p,tot}$ for the proposed cycle

According to Table 7, the highest COP_{ex} is 1.683 for R717 at point A with the worst economic performance of 72.19 $/h. The lowest $\dot{C}_{p,tot}$ is obtained by 2.905 $/h for R1234yf at point B with the worst exergetic performance of 0.654. At the optimum point, the maximum improvement in exergetic performance is achieved by 1.382 for R717 as the best refrigerant from the thermodynamic aspect. At this point COP_{ex} gets 2.37 times, $\dot{C}_{p,tot}$ is improved by 39.2% with respect to the base point and due to the similar trends of cost and EI performances, $\dot{B}_{p,tot}$ drops from 5.32 Pts/h to 3.22 Pts/h and COP_{en} rises from 3.21 to 5.86. In this case, the optimum operation parameters are 5°C, -28 °C and -49.9 °C of evaporating temperatures (i. e., T_{Ev1}, T_{Ev1} and T_{Ev3}, respectively), 30°C of condensing temperature, 0.484 of allocation ratio, and 0.884 kg/s of mass flow rate, respectively. Compared with the Pareto optimal solution of R290, R600a and R1234yf, respectively 7.3%, 10.6% and 39.7% more COP_{ex} are achieved. Meanwhile, at the optimum point, the highest improvement in $\dot{C}_{p,tot}$ is obtained by 52.6% for R1234yf which is the best refrigerant from the economic and EI viewpoints. At this point, $\dot{B}_{p,tot}$ reduces from 0.665 Pts/h to 0.313 Pts/h, the exergetic performance of the cycle gets 2 times and COP_{en} is improved from 2.84 to 5.63. As can be observed, the final optimum solutions for all refrigerants occur in the maximum T_{Ev1} and the minimum T_{Ev2}, T_{Ev3}, T_{CON} and φ within the defined ranges.

Table 7. Multi-objective optimization results for DETRC for all desired refrigerants.

Refrigerant	Point	COP$_{ex}$	$\dot{C}_{P,tot}$ ($/h)	$\dot{m}_1$ (kg/s)	φ	T$_{CON}$ (ºC)	T$_{Ev1}$ (ºC)	T$_{Ev2}$ (ºC)	T$_{Ev3}$ (ºC)
R717	A	1.683	72.19	1.588	0.488	30	5	-27.8	-42.6
	B	0.712	23.67	0.6	0.499	30	5	-10	-49.6
	Ideal point	1.672	23.65	-	-	-	-	-	-
	Non-ideal point	0.67	73.71	-	-	-	-	-	-
	Optimum point	1.382	39.52	0.884	0.484	30	5	-28	-49.9
	Optimum range	-	-	$0.6\leq\dot{m}_1$ ≤1.588	$0.48\leq\varphi$ ≤0.500	$30\leq T_{CON}\leq$ 30.6	$4.9\leq T_{Ev1}$ ≤5	$28\leq T_{Ev2}\leq$ -10	$50\leq T_{Ev3}\leq$ -26.2
R600a	A	1.483	22.77	1.764	0.480	30.3	5	-27.8	-50
	B	0.702	6.643	0.6	0.497	30.1	5	-10.1	-40.8
	Ideal point	1.487	6.639	-	-	-	-	-	-
	Non-ideal point	0.693	24.81	-	-	-	-	-	-
	Optimum point	1.249	11.95	0.958	0.483	30	5	-28	-49.8
	Optimum range	-	-	$0.6\leq\dot{m}_1$ ≤1.764	$0.48\leq\varphi$ ≤0.498	$30\leq T_{CON}\leq$ 30.3	~5	$28\leq T_{Ev2}\leq$ -10	$50\leq T_{Ev3}\leq$ -27.2
R290	A	1.53	23.55	1.821	0.48	30	5	-26.7	-49.9
	B	0.668	6.957	0.600	0.498	30.5	5	-10	-47.3
	Ideal point	1.535	6.949	-	-	-	-	-	-
	Non-ideal point	0.669	23.48	-	-	-	-	-	-
	Optimum point	1.288	12.77	1.002	0.48	30	5	-28	-50
	Optimum range	-	-	$0.6\leq\dot{m}_1$ ≤1.821	$0.48\leq\varphi$ ≤0.50	$30\leq T_{CON}\leq$ 30.5	~5	$28\leq T_{Ev2}\leq$ -10	$50\leq T_{Ev3}\leq$ -28.4
R1234yf	A	1.17	5.814	1.015	0.48	30.2	5	-28	-50
	B	0.654	2.905	0.600	0.50	30	5	-10.1	-50
	Ideal point	1.172	2.828	-	-	-	-	-	-
	Non-ideal point	0.653	5.941	-	-	-	-	-	-
	Optimum point	0.989	3.873	0.7128	0.480	30	5	-28	-49.2
	Optimum range	-	-	$0.6\leq\dot{m}_1$ ≤1.015	$0.48\leq\varphi$ ≤0.5	$30\leq T_{CON}\leq$ 30.2	$4.9\leq T_{Ev1}$ ≤5	$28\leq T_{Ev2}\leq$ -10	$50\leq T_{Ev3}\leq$ -27.8
Base point	R717	0.583	65.08						
	R600a	0.540	18.66	1	0.5	40	-2	-20	-30
	R290	0.544	18.41						
	R1234yf	0.495	8.186						

6. Conclusion

A novel triple-evaporator refrigeration cycle equipped with two-phase dual-nozzle ejector, called DETRC, is proposed to further reduction of throttling process losses. A mathematical model is developed to compare the performance of the proposed cycle with that of CETRC in order to demonstrate the superiority of DETRC. Then, the energy, exergy, exergoeconomic and exergoenvironmental concepts are applied to analyze and compare the performances of the proposed DETRC using low GWP

refrigerants (i.e., R717, R290, R600a, and R1234yf). In addition, the effect of major design parameters on the thermodynamic, cost and EI performances of the proposed cycle is assessed. Finally, a multi-objective optimization based on an evolutionary algorithm is used to find the optimum design parameters and performances of DETRC for all refrigerants. The results of this study indicate that:

- DETRC can perform much better in COP_{en} compared with CETRC at all given operating conditions because of the highest expansion work recovery potential of the two-phase dual-nozzle ejector.
- Using R717 in DETRC causes the maximum COP_{en} and COP_{ex} by 3.21 and 0.583, respectively and the lowest $\dot{C}_{p,tot}$ and $\dot{B}_{p,tot}$ are obtained by 8.186 \$/h and 0.665 Pts/h, respectively for R1234yf at the design operating conditions of T_{Ev1}=-2 °C, T_{Ev2}=-20 °C, T_{Ev3}=-30 °C , T_{CON}=40 °C and φ=0.5.
- Increasing T_{Ev1} improves the energy, exergy, economic and EI performances of DETRC, at the same time for all refrigerants owing to the reduction of compressor power and total exergy destruction rate. Based upon this, the COP_{en} and COP_{ex} of R717 are improved considerably by 2.87-4.19 and 0.527-0.743 and the total product cost and EI of R1234yf reduce by 9.1-6.33 \$/h and 0.74-0.51 Pts/h, respectively.
- With an increase of the ejector mass flow allocation ratio, R1234yf gives the lowest cost and EI performances with a range of 8.20-7.93 \$/h and 0.66-0.64 Pts/h, respectively for DETRC.
- The economic and environmental performances of DETRC are sharply affected by exergy destruction rate when R717 and R290 are used as refrigerants.

Applying the multi-objective optimization, the highest COP_{ex} and lowest total cost and EI performances of DETRC with corresponding optimum operating conditions are determined for all refrigerants. The final optimum performances are achieved when T_{Ev1} is close to the maximum value and T_{Ev2}, T_{Ev3}, T_{CON} and φ are close to the minimum values of the defined ranges.

References

[1] Bi, S., et al., Performance of a domestic refrigerator using TiO2-R600a nano-refrigerant as working fluid. Energy Conversion and Management, 2011. 52(1): p. 733-737.

[2] Fatouh, M. and M. El Kafafy, Assessment of propane/commercial butane mixtures as possible alternatives to R134a in domestic refrigerators. Energy Conversion and Management, 2006. 47(15-16): p. 2644-2658.

[3] Wongwises, S. and N. Chimres, Experimental study of hydrocarbon mixtures to replace HFC-134a in a domestic refrigerator. Energy conversion and management, 2005. 46(1): p. 85-100.

[4] Mohanraj, M., S. Jayaraj, and C. Muraleedharan, Environment friendly alternatives to halogenated refrigerants—A review. International Journal of Greenhouse Gas Control, 2009. 3(1): p. 108-119.

[5] Bolaji, B., Experimental study of R152a and R32 to replace R134a in a domestic refrigerator. Energy, 2010. 35(9): p. 3793-3798.

[6] Padilla, M., R. Revellin, and J. Bonjour, Exergy analysis of R413A as replacement of R12 in a domestic refrigeration system. Energy Conversion and Management, 2010. 51(11): p. 2195-2201.

[7] Padmanabhan, V.M.V. and S. Palanisamy, The use of TiO2 nanoparticles to reduce refrigerator ir-reversibility. Energy Conversion and Management, 2012. 59: p. 122-132.

[8] Sarkar, J., Ejector enhanced vapor compression refrigeration and heat pump systems—A review. Renewable and Sustainable Energy Reviews, 2012. 16(9): p. 6647-6659.

[9] Liu, Y., et al., Compression-injection hybrid refrigeration cycles in household refrigerators. Applied Thermal Engineering, 2010. 30(16): p. 2442-2447.

[10] Tomasek, M.-L. and R. Radermacher, Analysis of a domestic refrigerator cycle

with an ejector. 1995, American Society of Heating, Refrigerating and Air-Conditioning Engineers, Inc., Atlanta, GA (United States).

[11] Lin, C., et al., Pressure recovery ratio in a variable cooling loads ejector-based multi-evaporator refrigeration system. Energy, 2012. 44(1): p. 649-656.

[12] Chen, J., et al., A review on versatile ejector applications in refrigeration systems. Renewable and Sustainable Energy Reviews, 2015. 49: p. 67-90.

[13] Elakdhar, M., E. Nehdi, and L. Kairouani, Analysis of a compression/ejection cycle for domestic refrigeration. Industrial & engineering chemistry research, 2007. 46(13): p. 4639-4644.

[14] Lawrence, N. and S. Elbel, Theoretical and practical comparison of two-phase ejector refrigeration cycles including First and Second Law analysis. International Journal of Refrigeration, 2013. 36(4): p. 1220-1232.

[15] Elakhdar, M., et al., Thermodynamic analysis of a novel Ejector Enhanced Vapor Compression Refrigeration (EEVCR) cycle. Energy, 2018. 163: p. 1217-1230.

[16] Chen, Q., G. Yan, and J. Yu, Performance analysis of an ejector enhanced refrigeration cycle with R290/R600a for application in domestic refrigerator/freezers. Applied Thermal Engineering, 2017. 120: p. 581-592.

[17] Wang, X., et al., Comparative studies of ejector-expansion vapor compression refrigeration cycles for applications in domestic refrigerator-freezers. Energy, 2014. 70: p. 635-642.

[18] Yu, J., X. Song, and M. Ma, Theoretical study on a novel R32 refrigeration cycle with a two-stage suction ejector. International Journal of Refrigeration, 2013. 36(1): p. 166-172.

[19] Zhou, M., X. Wang, and J. Yu, Theoretical study on a novel dual-nozzle ejector enhanced refrigeration cycle for household refrigerator-freezers. Energy conversion and management, 2013. 73: p. 278-284.

[20] Kairouani, L., et al., Use of ejectors in a multi-evaporator refrigeration system for performance enhancement. International Journal of Refrigeration, 2009. 32(6): p. 1173-1185.

[21] Calm, J.M. and G.C. Hourahan. Physical, safety, and environmental data for current and alternative refrigerants. in Proceedings of 23rd International Congress of Refrigeration (ICR2011), Prague, Czech Republic, August. 2011.

[22] Li, H., et al., Performance characteristics of R1234yf ejector-expansion refrigeration cycle. Applied energy, 2014. 121: p. 96-103.

[23] Sayyaadi, H. and M. Nejatolahi, Multi-objective optimization of a cooling tower assisted vapor compression refrigeration system. international journal of refrigeration, 2011. 34(1): p. 243-256.

[24] He, S., Y. Li, and R. Wang, Progress of mathematical modeling on ejectors. Renewable and Sustainable Energy Reviews, 2009. 13(8): p. 1760-1780.

[25] Li, D. and E.A. Groll, Transcritical CO2 refrigeration cycle with ejector-expansion device. International Journal of refrigeration, 2005. 28(5): p. 766-773.

[26] Zhu, L., et al., Performance analysis of a novel dual-nozzle ejector enhanced cycle for solar assisted air-source heat pump systems. Renewable Energy, 2014. 63: p. 735-740.

[27] Bejan, A. and G. Tsatsaronis, Thermal design and optimization. 1996: John Wiley & Sons.

[28] Tsatsaronis, G., Definitions and nomenclature in exergy analysis and exergoeconomics. Energy, 2007. 32(4): p. 249-253.

[29] Aminyavari, M., et al., Exergetic, economic and environmental (3E) analyses, and multi-objective optimization of a CO2/NH3 cascade refrigeration system. Applied Thermal Engineering, 2014. 65(1-2): p. 42-50.

[30] Morosuk, T., G. Tsatsaronis, and C. Koroneos, Environmental impact reduction using exergy-based methods. Journal of Cleaner Production, 2016. 118: p. 118-123.

[31] Meyer, L., et al., Exergoenvironmental analysis for evaluation of the environmental impact of energy conversion systems. Energy, 2009. 34(1): p. 75-89.

[32] Cavalcanti, E.J.C., Exergoeconomic and exergoenvironmental analyses of an integrated solar combined cycle system. Renewable and Sustainable Energy Reviews, 2017. 67: p. 507-519.

[33] Deb, K., et al., A fast and elitist multiobjective genetic algorithm: NSGA-II. IEEE transactions on evolutionary computation, 2002. 6(2): p. 182-197.

[34] Zitzler, E., K. Deb, and L. Thiele, Comparison of multiobjective evolutionary algorithms: Empirical results. Evolutionary computation, 2000. 8(2): p. 173-195.

[35] Feng, Y., et al., Comparison between regenerative organic Rankine cycle (RORC) and basic organic Rankine cycle (BORC) based on thermoeconomic multi-objective optimization considering exergy efficiency and levelized energy cost (LEC). Energy Conversion and Management, 2015. 96: p. 58-71.

[36] Konak, A., D.W. Coit, and A.E. Smith, Multi-objective optimization using genetic algorithms: A tutorial. Reliability Engineering & System Safety, 2006. 91(9): p. 992-1007.

[37] Li, Y., S. Liao, and G. Liu, Thermo-economic multi-objective optimization for a solar-dish Brayton system using NSGA-II and decision making. International Journal of Electrical Power & Energy Systems, 2015. 64: p. 167-175.